Engineering and Technology Journal
Journal homepage: https://etj.uotechnology.edu.iq

# Enhancing antibacterial performance of powder metallurgy-fabricated Ti, Ti-15Mo, and Ti-45Zr alloys through small liquid metal gallium additions in biomedical applications

**Ammar R. Hasan**[a,b]*, **Fatimah J. Al-Hasani**[b], **Emad S. Al-Hassani**[b]

[a] Materials Engineering Department, Faculty of Engineering, University of Kufa, Iraq.
[b] Materials Engineering Dept., University of Technology-Iraq, Alsina'a street, 10066 Baghdad, Iraq.
*Corresponding author Email: ammarr.alshemary@uokufa.edu.iq

## HIGHLIGHTS

- Molds were designed and implemented for sample fabrication using powder metallurgy at 10, 15, and 30 mm.
- Alloys were fabricated by powder metallurgy from Ti, Ti-15Mo, and Ti-45Zr as reference materials.
- New alloys were made by mixing Ti, Ti-15Mo, and Ti-45Zr with 1–2.5% gallium using powder metallurgy.
- Gallium (1–2.5%) improved antibacterial activity of Ti, Ti-15Mo, and Ti-45Zr alloys.
- Gallium (1–2.5%) enhanced antiproliferative activity without cytotoxicity in the tested alloys.

**Keywords:**
Gallium
Titanium
Titanium-15 Molybdenum
Titanium-45 Zirconium
Powder Metallurgy
Antibacterial Activity
Biomaterial

## ABSTRACT

This study investigates the influence of small liquid metal gallium additions (1, 1.5, 2, and 2.5 wt%) on the antibacterial performance of Ti, Ti-15Mo, and Ti-45Zr alloys fabricated by the powder metallurgy method. The alloys were manufactured by sintering at 1250 °C to improve the antibacterial activity of Titanium and its alloys in biomaterial applications. X-ray diffraction (XRD) was used to identify the dominant compounds and phases after adding liquid gallium metal, and the antibacterial activity was also tested; the results indicate an increase in the Zone of inhibition of Ti, Ti-15Mo, and Ti-45Zr with increasing gallium/Ga content, where the Zone of inhibition increased by approximately 12, 12.5 and 18% for Ti, Ti-15Mo, and Ti-45Zr, respectively. This is attributed to $Ga^{3+}$, which disrupts iron-dependent enzymes and metabolic pathways (e.g., DNA synthesis, electron transport), inhibiting bacterial growth. Adding Ga alters the alloy's surface topography and chemistry, reducing bacterial adhesion. A smoother or more hydrophobic surface prevents bacterial colonization and biofilm formation. Titanium and its alloys with liquid gallium metal were also shown to be non-toxic biomaterials with biocompatibility properties for MCF-10 cells. Ga additives for Ti, Ti-15Mo, and Ti-45Zr improve antibacterial performance, making these alloys promising for medical implants and reducing infection risks without relying on antibiotics. Further optimization of Ga concentration and release kinetics is critical to balance efficacy and biocompatibility.

## 1. Introduction

Titanium and its alloys are widely employed in hard tissue applications in dentistry and total joint replacements, including hip, knee, and spinal surgeries, due to their superior corrosion resistance and exceptional biocompatibility compared to other metallic implant materials, such as cobalt-chromium and austenitic stainless steel [1]. Nonetheless, the current biomedical Titanium and its alloys possess limitations that may result in implant failure. These alloys demonstrate superior elastic moduli compared to cortical bone. The discrepancy between the implant and the adjacent bone results in aseptic loosening of load-bearing implants, referred to as the stress-shielding phenomenon [2]. Furthermore, current research has identified the emergence of health diseases resulting from the discharge of metallic ions, such as aluminum and vanadium, into adjacent tissues and the bloodstream [3]. A significant factor in implant failure is biomaterial-associated infection, which is thought to occur when bacterial biofilms form on implant surfaces and the innate immune response fails to eradicate them [4].

Furthermore, bacteria within biofilms are challenging to treat due to their heightened susceptibility to antibiotics relative to their planktonic (free-floating) counterparts [5]. The development of biofilms on Titanium and its alloys can be obstructed by coating or alloying the implant with inorganic antibacterial agents, such as zinc, silver, copper, and gallium [6]. Gallium-based compounds exhibit antibacterial efficacy against infections induced by multidrug-resistant ESKAPE pathogens (Enterococcus



http://doi.org/10.30684/etj.2025.160012.1954
Received 01 June 2025; Received in revised form 26 June 2025; Accepted 03 July 2025; Available online 25 September 2025
2412-0758/University of Technology-Iraq, Baghdad, Iraq

faecium, Staphylococcus aureus, Klebsiella pneumoniae, Pseudomonas aeruginosa, and Enterobacter species) as well as P. aeruginosa biofilms [7]. Gallium can reduce bacterial survival and biofilm formation on implant surfaces without antibiotics by releasing Fenton-active Fe into the cytoplasm, thereby generating reactive oxygen species [8]. In addition to the necessary antibacterial effectiveness, modifications to biomaterial surfaces must preserve superior biocompatibility with host cells and tissues while improving the host immune response [9].

In recent years, significant research and development have been aimed at improving the properties and applications of these materials in the medical industry. Titanium and its alloys have many applications in the human body, including dental implants, orthopedic implants, and cardiovascular devices [10]. Several studies have reported that adding Ga or other metals to Titanium and its alloys can improve their corrosion behavior, mechanical properties, and antibacterial performance. Yamaguchi et al. [11], explored the antibacterial activity of Ga-Ti alloy. It highlighted the high antibacterial activity possessed by the material towards A. baumannii, and its improved bioactivity. Cochis et al. [12], demonstrated that metallurgical addition of Ga, even in small amounts (1−2%) to titanium alloys, has a highly efficient antibacterial function without any visible cytotoxic effect. Vishnu et al. [13] investigated the development of β-Ti-Nb alloys enriched with small additions of gallium (Ga) or copper (Cu) to achieve an antimicrobial property to prevent infections. The Ti–Nb–Ga alloys recorded activity of ~80–95% against S. aureus and E. coli due to the effect of $Ga^{3+}$, which inhibits bacterial growth by inactivating iron. The Cu alloys achieved bacterial killing rates of ≥90% due to $Ti_2Cu$, which operates on contact without releasing toxic ions, with appropriate heat treatment. Analysis of cell effects (e.g., bone cells) demonstrated low cytotoxicity for $Ga^{3+}$ or $Cu^{2+}$ ions at the concentrations used. The research emphasized that antibacterial activity does not compromise cytocompatibility, enhancing the alloy's feasibility in bio-based applications. Alberta et al. [14], prepared three novel β-type (Ti–45Nb)-based alloys with minor additions of the antibacterial elements Ga and Cu $(Ti\text{-}45Nb)_{96}$-4Ga, $(Ti\text{-}45Nb)_{96}$-4Cu, and $(Ti\text{-}45Nb)_{96}$-2Ga-2Cu wt.%) by a two-step casting process followed by homogenization treatment. The research characterized the alloys' microstructure, phase composition, mechanical properties, corrosion behavior, and antibacterial activity. The research found that the Ga and Cu additions refine the grain size and increase the fraction of β phase in the alloys. The study also found that the Ga and Cu additions improve the alloys' corrosion resistance and antibacterial activity but reduce their strength and modulus. McHendrie et al. [15], reported that the antibacterial assay depicted that Ga-coated samples prevented bacterial colony formation of S. aureus and exhibited enhanced antimicrobial action. Li et al. [16] demonstrated that Ti-Ga alloys offer a promising dual-function approach to bone implants, simultaneously preventing bacterial biofilm formation and inhibiting osteoclast-mediated bone resorption by targeting iron metabolism. Biofilm biomass-biofilm formation on Ti-Ga surfaces was reduced to ~1.7% for S. aureus and ~2.0% for E. coli compared to pure Ti controls. This strategy addresses the leading causes of implant failure and may significantly improve clinical outcomes.

Recently, the incorporation of Ga into Ti alloys has received significant attention due to its proven antibacterial properties and potential to enhance corrosion resistance. However, most previous studies have been conducted on binary Ti-Ga systems or Ti alloys containing components such as Mo, Ta, and Nb. The use of Ga in the Ti-45Zr system is largely unknown, particularly in powder metallurgy. This manufacturing method offers improved control over microstructure and phase distribution, enabling more precise tailoring of mechanical and biological properties. This study presents minor additions of Ga to binary Ti-45Zr alloys produced using powder metallurgy, to evaluate their combined effects on antibacterial efficacy and structural properties in biomedical applications. The production process utilizing powder metallurgy between solid titanium powder and liquid gallium metal sets this study apart from earlier studies. Powder metallurgy technology is distinguished by its capacity to produce alloys and components with high efficiency, precision, and adaptability, particularly for intricate geometries and tailored material properties. Its benefits in terms of material use, design versatility, and the capacity to create novel materials make it an essential technology in contemporary production, especially in sophisticated and high-volume applications. The research aims to improve the antibacterial performance of Titanium and its alloys in biomedical applications through small additions of liquid gallium metal fabricated using powder metallurgy.

## 2. Materials and methods

### 2.1 Materials

Pure Titanium is a lustrous transition metal with a silver color, low density, and high strength. It is resistant to corrosion in seawater and chlorine. The Titanium used is a powder with a purity of up to 99.8% imported from Fluka Company (brand name of Honeywell Research Chemicals) in Morris Plains, New Jersey, USA.

Pure molybdenum is a silvery-grey metal with a high melting point and a low coefficient of thermal expansion. The molybdenum used is a powder with a purity of up to 99.9% imported from SkySpring Nanomaterials, Inc. in Houston, Texas, USA. Pure zirconium is a chemical element with the symbol Zr and atomic number 40. It is a lustrous, greyish-white, soft, ductile, malleable metal highly resistant to corrosion by alkalis, acids, salt water, and other agents. The zirconium used is a powder with a purity of up to 99.9% imported from Nanochemazone Company in Saskatoon, Saskatchewan, Canada. Pure gallium is a silvery blue metal that fractures conchoidally like glass. Its very low melting point is 29.76 °C (85.57 °F), which means it can melt in your hand. The gallium used is a liquid metal with a purity of up to 99.9% imported from Fluka Chemie GmbH in Buchs, Switzerland.

### 2.2 Preparation of samples by powder metallurgy

Alloy powders were prepared by mixing (blending) the powders in a mixing machine according to the following mixing process conditions, as shown in Table 1. The metal powder (Ti) was prepared according to the following proportions and weights

as shown in Table 2. The alloy powder (Ti-15Mo) was prepared according to the following proportions and weights as shown in Table 3. The alloy powder (Ti-45Zr) was prepared according to the following proportions and weights as shown in Table 4.

Addition of the liquid metal Gallium (Ga) to metal powder (Ti) and Alloy powders (Ti-15Mo\Ti-45Zr) by mixing the powder and Gallium (Ga) in a mixing machine according to the following mixing process conditions, as shown in Table 1.

Liquid metal gallium (Ga) was added to the metal powder (Ti), which was prepared according to the following proportions and weights, as shown in Table 5.

Liquid metal gallium (Ga) was added to the alloy powder (Ti-15Mo), which was prepared according to the following proportions and weights, as shown in Table 6.

Adding liquid metal Gallium (Ga) to the alloy powder (Ti-45Zr) was prepared according to the proportions and weights in Table 7. After adding liquid metal Gallium (Ga) to alloy powders, they are annealed at room temperature and in sunlight to increase the chemical reaction between gallium liquid metal and other powders. The following conditions are shown in Table 8.

**Table 1:** Processing conditions for mixing

| Parameter | Condition |
|---|---|
| Mixing time | 3h |
| Rotation rate | 100 rpm |
| Ball-to-powder ratio | 4:1 |
| Ball size and type | 5 mm-10 mm\Tungsten Carbide |
| Container size and type | \Tungsten Carbide |

**Table 2:** Proportions and weights of metal powder (Ti)

| According to | Ti |
|---|---|
| Proportions (%) | 100 |
| Weights (gm) | 100 |

**Table 3:** Proportions and weights of alloy powder (Ti-15Mo)

| According to | Ti | Mo | Ti-15Mo |
|---|---|---|---|
| Proportions (%) | 85 | 15 | 100 |
| Weights (gm) | 85 | 15 | 100 |

**Table 4:** Proportions and weights of powder alloy (Ti-45Zr)

| According to | Ti | Zr | Ti-45Zr |
|---|---|---|---|
| Proportions (%) | 55 | 45 | 100 |
| Weights (gm) | 55 | 45 | 100 |

**Table 5:** Proportions and weights of metal powder Ti with (Ga)

| According to | Ti | | | | |
|---|---|---|---|---|---|
| Proportions (%) | 100 | 99 | 98.5 | 98 | 97.5 |
| Weights (gm) | 20 | 19.8 | 19.7 | 19.6 | 19.5 |
| **According to** | **Ga** | | | | |
| Proportions (%) | 0 | 1 | 1.5 | 2 | 2.5 |
| Weights (gm) | 0 | 0.2 | 0.3 | 0.4 | 0.5 |
| **According to** | **Ti-XGa** | | | | |
| Proportions (%) | 100 | 100 | 100 | 100 | 100 |
| Weights (gm) | 20 | 20 | 20 | 20 | 20 |

**Table 6:** Proportions and weights of alloy powder (Ti-15Mo) with (Ga)

| According to | Ti | | | | |
|---|---|---|---|---|---|
| Proportions (%) | 100 | 99 | 98.5 | 98 | 97.5 |
| Weights (gm) | 20 | 19.8 | 19.7 | 19.6 | 19.5 |
| **According to** | **Ga** | | | | |
| Proportions (%) | 0 | 1 | 1.5 | 2 | 2.5 |
| Weights (gm) | 0 | 0.2 | 0.3 | 0.4 | 0.5 |
| **According to** | **Ti-15Mo-XGa** | | | | |
| Proportions (%) | 100 | 100 | 100 | 100 | 100 |
| Weights (gm) | 20 | 20 | 20 | 20 | 20 |

**Table 7:** Proportions and weights of alloy powder (Ti-45Zr) with (Ga)

| **According to** | **Ti** | | | | |
|---|---|---|---|---|---|
| Proportions (%) | 100 | 99 | 98.5 | 98 | 97.5 |
| Weights (gm) | 20 | 19.8 | 19.7 | 19.6 | 19.5 |
| **According to** | **Ga** | | | | |
| Proportions (%) | 0 | 1 | 1.5 | 2 | 2.5 |
| Weights (gm) | 0 | 0.2 | 0.3 | 0.4 | 0.5 |
| **According to** | **Ti-45Zr-XGa** | | | | |
| Proportions (%) | 100 | 100 | 100 | 100 | 100 |
| Weights (gm) | 20 | 20 | 20 | 20 | 20 |

**Table 8:** Annealing conditions

| **Parameter** | **Condition** |
|---|---|
| Annealing time | More than (5) days |
| Annealing temperature | (35-45) ℃ |

Then, the quantity of powders used for each sample will be weighed. The powder's weight can be determined through the size of the sample to be manufactured and the density of the powder.

The formula 1 gives the volume of a cylinder:

$$V=\pi r^2 h \quad (1)$$

where: V is the volume of a cylinder ($mm^3$), r is the radius (m), h is the height (m).

By using this formula, we can calculate the volume of each sample.

The formula 2 gives the weight of each sample:

$$W=\rho V \quad (2)$$

where: W is the weight of the sample (mg), ρ is the density ($mg/mm^3$), V is the volume ($mm^3$).

By using this formula, we can calculate the weight of each sample. The weight of powders used for each sample is shown in Table 9.

**Table 9:** Weigh the quantity of powders used for each sample

| **Size** | **Ti** |
|---|---|
| (10*5) $mm^2$ | 1.76 g |
| (15*7) $mm^2$ | 5.56 g |
| (30*3) $mm^2$ | 9.54 g |

Then weigh the required quantity of powder; lubricate the mold (die) and fill the die cavities with the required amount of powder. Alloy powder pressing (compaction) is done using a hydraulic press machine. Under the following conditions, as shown in Table 10, the required compact density of the samples can be obtained.

**Table 10:** Pressing conditions

| **Parameter** | **Condition** |
|---|---|
| Compaction load (ton) | 20 |
| Time hold (min) | 5 |

Then, compact (Green parts) anneal at room temperature and sunlight to complete the chemical reaction between gallium metal and other elements in the green parts under the following conditions, shown in Table 8. Green parts (Compact) sintering at an argon gas tube furnace type (GSL-1500X). Argon is nonflammable and inert, and is used as a backfill in the furnace. Under the following conditions shown in Table 11, sintering at stepped temperatures before the high hold grade is necessary to remove the pressing lubricant and prevent cracking due to expansion and thermal shock.

**Table 11:** Sintering conditions

| **Parameter** | **Temperature (ºC)** | **Time (hold) (min)** |
|---|---|---|
| $Step_1$Temperature | 250 | 15 |
| $Step_2$ Temperature | 500 | 15 |
| Sintering Temperature | 1250 | 90-120 |

Then prepare the samples by grinding their surfaces using Grind paper (100, 180, 240, 320, 400, 600, 800, 1000, 1200). Figure 1 shows the shape of the samples after the Grinding process.

**Figure 1:** Shows the shape of the samples after the grinding process

Final samples were manufactured according to different gallium percentages as shown in Table 12.

**Table 12:**Final manufactured samples for Ti-XGa

| Sample No. | Ti-XGa |
|---|---|
| 1 | Ti |
| 2 | Ti-1Ga |
| 3 | Ti-1.5Ga |
| 4 | Ti-2Ga |
| 5 | Ti-2.5Ga |
| 6 | Ti-15Mo |
| 7 | (Ti-15Mo)-1Ga |
| 8 | (Ti-15Mo)-1.5Ga |
| 9 | (Ti-15Mo)-2Ga |
| 10 | (Ti-15Mo)-2.5Ga |
| 11 | Ti-45Zr |
| 12 | (Ti-45Zr)-1Ga |
| 13 | (Ti-45Zr)-1.5Ga |
| 14 | (Ti-45Zr)-2Ga |
| 15 | (Ti-45Zr)-2.5Ga |

## 2.3 Sample examination

### 2.3.1 Characterization

The samples' XRD test was conducted using an XRD device manufactured by Thermo Scientific, USA.

### 2.3.2 Antibacterial test

The Inhibition Zone method was employed to assess the antibacterial efficacy of samples. The Zone of Inhibition Test, often referred to as the Kirby-Bauer Test, Antimicrobial Susceptibility Test, Disk Diffusion Test, or Agar Diffusion Test, is a rapid and cost-effective method for evaluating the antimicrobial efficacy of a substance or solution against a specific pathogen. If the bacterial or fungal strain is responsive to the antimicrobial treatment, a clear zone indicating microbial growth inhibition will manifest on the agar plate. If it exhibits resistance to the antimicrobial treatment, then growth remains unaffected, and no distinct zone is observable. The bacterial species Staphylococcus aureus (S. aureus) was used as the model microorganism. The antibacterial efficacy of the produced samples was assessed against Gram-negative and Gram-positive bacterial strains utilizing the agar well diffusion assay [17, 18]. Approximately 20 mL of Muller–Hinton (MH) agar was aseptically dispensed into sterile Petri dishes. The bacterial species were obtained from their stock cultures utilizing a sterile wire loop [19]. Following the cultivation of the organisms, 6 mm-diameter epoxy was applied to the agar plates. The cultivated plates with the samples and test organisms were incubated for 24 hours at 37 °C before measuring and documenting the diameters of the inhibition [20,21].

Muller-Hinton (M-H) was made by dissolving 38 grams of Beef Extract Powder in 1 liter of distilled water, then heating on a burner with agitation. M-H requires autoclaving for 15 minutes at 121 °C for sterilization. The mixture was permitted to cool to 50 °C before being poured into a petri dish and left for approximately 15 minutes to solidify, after which it was inverted and stored in the refrigerator at 4 °C.

### 2.3.3 MTT assay (Cytotoxicity assay)

Maintenance of cell cultures: The MCF-10 cell line was cultured in RPMI-1640 enriched with 10% fetal bovine serum, 100 units/mL penicillin, and 100 µg/mL streptomycin. Cells were subcultured using trypsin-EDTA, reseeded at 80% confluence biweekly, and incubated at 37 °C [22, 23]. The MTT assay was conducted using 96-well plates to evaluate the cytotoxic effect of samples 3, 9, and 14, which possess superior mechanical properties and good antibacterial activity [24, 25]. Cell lines were

inoculated at a density of 1 × $10^4$ cells per well after 24 hours. Alternatively, a confluent monolayer was established, and MCF-10 cells were treated with samples 3, 9, and 14. After 72 hours of treatment, cell viability was assessed by discarding the medium, introducing 100 µL of 2 mg/mL MTT, and incubating the cells for 2.5 hours at 37 °C. After removing the MTT solution, the crystals in the wells were solubilized by adding 130 µL of DMSO (Dimethyl Sulphoxide), followed by a 15-minute incubation at 37 °C with agitation [26]. The absorbance was measured using a microplate reader at 492 nm; the test was conducted in triplicate. The cell growth inhibition rate (cytotoxicity percentage) was determined using the subsequent Equation 3 [27,28]:

$$\text{Inhibition rate (Cytotoxicty \%)} = \frac{A-B}{A} \times 100 \quad (3)$$

where: A is the absorbance of the control, B is the absorbance of the tested sample.

The obtained data were statistically analyzed using an unpaired t-test with GraphPad Prism 10. The values were presented as the mean ± SD of triplicate measurements.

## 3. Results and discussion

### 3.1 XRD test

The XRD data for Ti-XGa shown in Figure 2 indicates that the main phase of the Ti metal was the α phase (hexagonal close-packed structure). The atomic radius of Ti is 147 picometers (pm) or 1.47 angstroms (A°), while the atomic radius of Ga is 135 pm or 1.35 A°. Adding liquid gallium metal in small proportions enhances the stability of the α-phase and the appearance of the α'-phase. The appearance of the α' phase (hexagonal close-packed structure) in titanium alloys usually indicates a martensitic transformation from the beta phase upon cooling. However, when gallium is added to Titanium, it primarily acts as α α-phase stabilizer and lowers the α to β phase transition temperature (223 °C). This may increase the formation of beta-related phases such as the α' phase. In addition to the appearance of intermetallic compounds, $Ti_3Ga$ and $TiGa_3$.

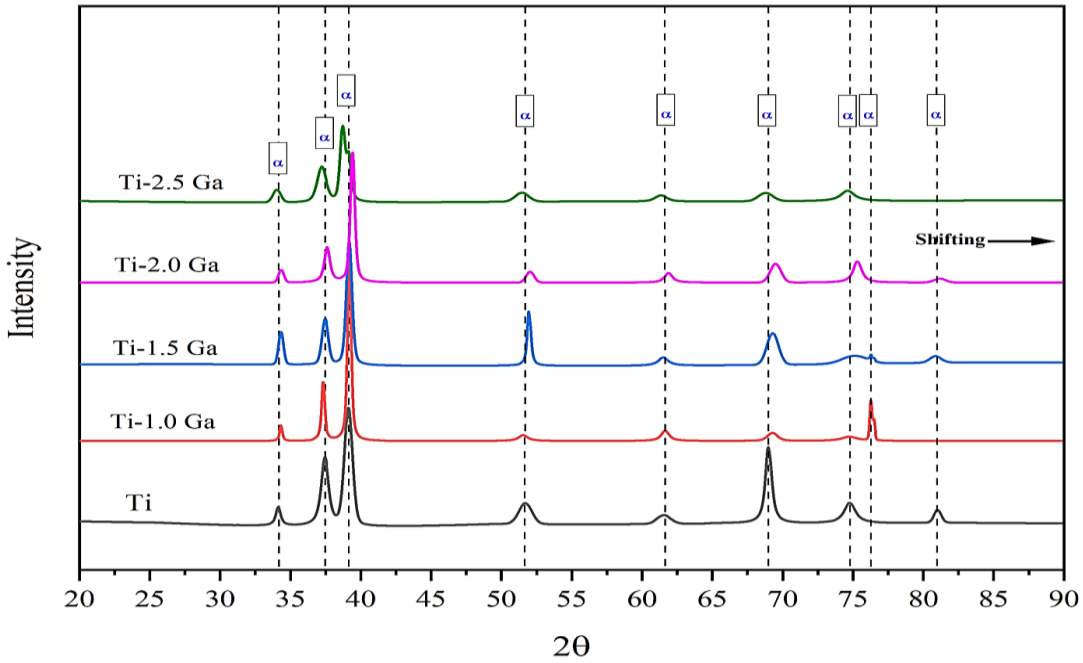


**Figure 2:** XRD Test for Ti-XGa

To determine the phase and intermetallic ratios resulting from adding a variable content of Ga (1-2.5 wt%) to Ti metal using metal powder, based on XRD patterns using (Rietveld purification), and using (FullProf) software, the results appeared as shown in Table 13.

**Table 13:** Phase and intermetallic ratios for Ti–XGa

| Sample | Phase | wt% (±1.5%) | Crystal Structure |
|---|---|---|---|
| Ti | α-Ti | 100% | HCP |
| Ti–1Ga | α-Ti | 100% | HCP |
| Ti–1.5Ga | α-Ti | 98% | HCP |
| | $Ti_3Ga$, $TiGa_3$ | 2% | Intermetallic |
| Ti–2Ga | α-Ti | 96% | HCP |
| | $Ti_3Ga$, $TiGa_3$ | 4% | Intermetallic |
| Ti–2.5Ga | α-Ti | 92% | HCP |
| | $Ti_3Ga$, $TiGa_3$ | 8% | Intermetallic |

The XRD data for (Ti-15Mo)-XGa shown in Figure 3 indicates that the main phases of the Ti-15Mo alloy were the α phase (hexagonal close-packed structure), β-phase (body-centered cubic structure), and (α; β)-phase. The atomic radius of Ti (147 pm) or (1.47 A°) and the atomic radius of Mo (139 pm) or (1.39 A°) are different from the atomic radius of Ga (135 pm) or (1.35 A°). The Ti-15Mo alloy is a β (beta)-stabilized titanium alloy. Molybdenum (Mo) acts as a strong β-phase stabilizer retained at room temperature because Mo significantly lowers the β-phase transition temperature. Adding liquid gallium metal in small proportions enhances the stability of the β-phase and the appearance of the α'-phase or β'-phase. In addition to the appearance of intermetallic compounds $Ti_5Ga_3$, $Ti_5Ga_4$, and $Ti_3Ga$.

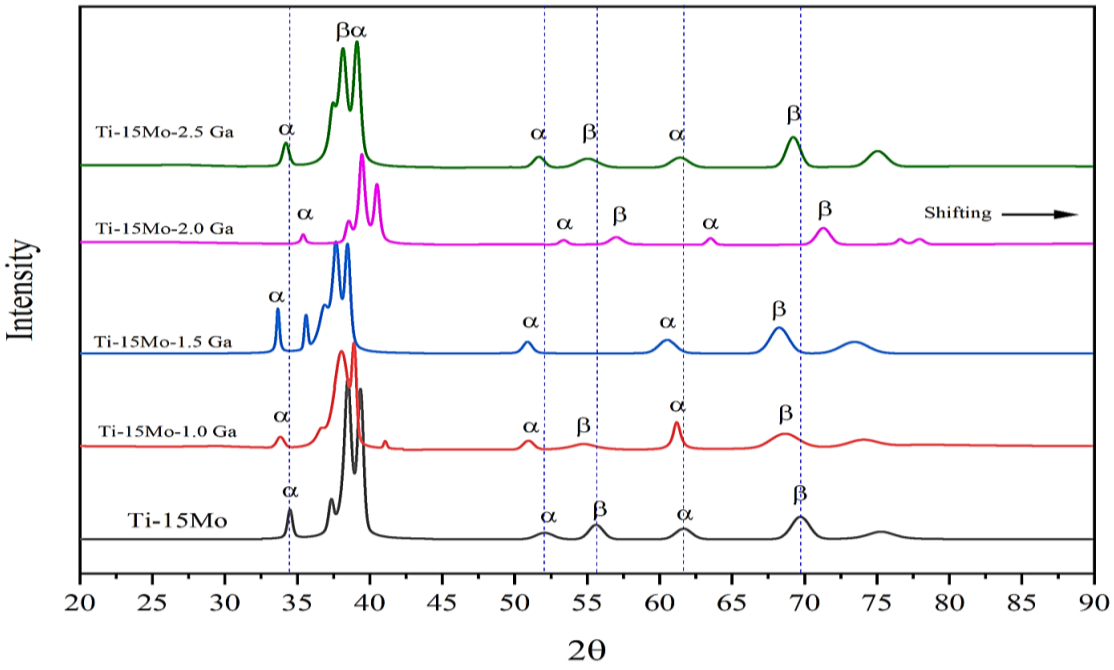


**Figure 3:** XRD Test for (Ti-15Mo)-XGa

To determine the phase and intermetallic ratios resulting from adding a variable content of Ga (1-2.5 wt%) to Ti-15Mo alloy using metal powder, based on XRD patterns using (Rietveld purification), and using (FullProf) software, the results appeared as shown in Table 14.

**Table 14:** Phase and intermetallic ratios for (Ti-15Mo)–XGa

| Sample | Phase | wt% (±1.5%) | Crystal Structure |
|---|---|---|---|
| Ti–15Mo | α-Ti | 36 | HCP |
| | β-Ti | 64 | BCC |
| (Ti–15Mo)–1Ga | α-Ti | 42 | HCP |
| | β-Ti | 58 | BCC |
| (Ti–15Mo)–1.5Ga | α-Ti | 48 | HCP |
| | β-Ti | 50 | BCC |
| | $Ti_3Ga$ | 2 | Intermetallic |
| (Ti–15Mo)–2Ga | α-Ti | 52 | HCP |
| | β-Ti | 44 | BCC |
| | $Ti_5Ga_3$ | 4 | Intermetallic |
| (Ti–15Mo)–2Ga | α-Ti | 56 | HCP |
| | β-Ti | 40 | BCC |
| | $Ti_5Ga_4$ | 4 | Intermetallic |

The XRD data for (Ti-45Zr)-XGa shown in Figure 4 indicates that the main phases of the Ti-45Zr alloy were the α phase (hexagonal close-packed structure), α`phase (hexagonal close-packed structure), and β-phrase (body-centered cubic structure). The atomic radius of Ti (147 pm) or (1.47 A°) and the atomic radius of Zr (160 pm) or (1.39 A°) are different from that of Ga (135 pm) or (1.35 A°). The Ti-30Ta alloy is an α-stabilized titanium alloy but has potential for α'-martensite (distorted HCP) and β-phase if quenched from the β-phase region, though rare in Ti-Zr alloys. Ti and Zr form a continuous solid solution in both α and β phases due to their similar atomic radii and crystal structures. For Ti-45Zr, the β transition lies between the pure Ti (882 °C) and pure Zr (863 °C) values (~865–870 °C). Adding liquid gallium metal in small proportions enhances the stability of the α-phase and the α' -phase or β-phase. No intermediate compounds form because the system is purely substituted.

To determine the phase and intermetallic ratios resulting from adding a variable content of Ga (1-2.5 wt%) to Ti-45Zr alloy using metal powder, based on XRD patterns using (Rietveld purification), and using (FullProf) software, the results appeared as shown in Table 15.

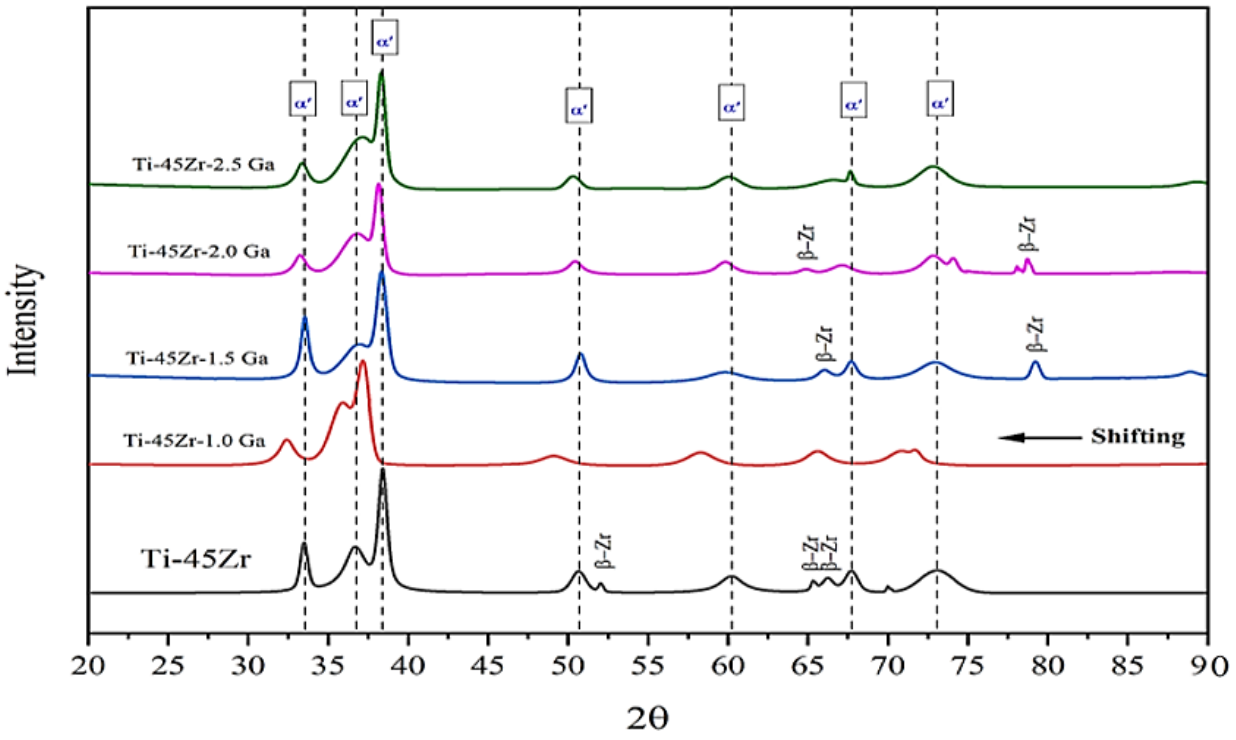


**Figure 4:** XRD Test for (Ti-45Zr)-XGa

**Table 15:** Phase and intermetallic ratios for (Ti-45Zr)–XGa

| Sample | Phase | wt% (±1.5%) | Crystal Structure |
|---|---|---|---|
| Ti–45Zr | α, α′-Ti | 42% | HCP |
| | β-Ti | 58% | BCC |
| (Ti–45Zr)–1Ga | α, α′-Ti | 51% | HCP |
| | β-Ti | 49% | BCC |
| (Ti–45Zr)–1.5Ga | α-Ti | 56% | HCP |
| | β-Ti | 42% | BCC |
| | $Ti_{1.34}Zr_{0.66}$ | 2% | Intermetallic |
| (Ti–45Zr)–2Ga | α, α′-Ti | 60% | HCP |
| | β-Ti | 38% | BCC |
| | $Ti_{1.34}Zr_{0.66}$ | 2% | Intermetallic |
| (Ti–45Zr)–2.5Ga | α, α′-Ti | 65% | HCP |
| | β-Ti | 34% | BCC |
| | $Ti_{1.34}Zr_{0.66}$ | 1% | Intermetallic |

## 3.2 Antibacterial test

Metallic implants are prone to bacterial infection, potentially resulting in severe repercussions for patients. Bacteria can attach to the implant surface, proliferate, and establish a biofilm. Conventional Titanium and its alloys lack natural antibacterial properties; however, liquid gallium metal has been used to alter their surface characteristics, thereby preventing biofilm development by blocking the initial stage of infection, specifically bacterial adherence. Creating biomaterials that resist bacterial infection poses a significant challenge in orthopedics and dentistry. This is particularly crucial for patients with weakened immune systems, such as individuals with diabetes or cancer, who face an elevated risk of infection. Infection may necessitate many surgical procedures, amputation, or result in mortality.

Improving the antibacterial performance of Ti-Ga alloys makes them promising for medical implants. These alloys can reduce infection risks without relying on antibiotics. Further optimization of Ga concentration and release kinetics is critical to balancing efficacy and biocompatibility. This study is among the initial systematic examinations of Ga-modified Ti-45Zr alloys produced via powder metallurgy. Although Ga has demonstrated the capacity to enhance the antibacterial properties of several titanium alloys, its interaction with high-zirconium alloys is inadequately explored in scientific literature. The current findings indicate that the incorporation of Ga facilitates the development of intermetallic complexes and stabilizes the beta phase, enhancing antibacterial activity and surface characteristics. This highlights the innovation and promise of employing Ga in Ti-45Zr-based biomaterials, particularly considering the biocompatibility and superior mechanical properties of the Ti-45Zr system. Table 16 and Figure 5 show the effect of adding gallium to Ti metal in proportions of 1, 1.5, 2, and 2.5% by powder metallurgy method on antibacterial activity (Zone of inhibition).

**Table 16:** Shows the effect of adding Ga to Ti metal on the zone of inhibition

| | Sample No. | Zone of inhibition (mm) |
|---|---|---|
| S. aureus | 1 | 25 |
| | 2 | 27 |
| | 3 | 27 |
| | 4 | 28 |
| | 5 | 28 |

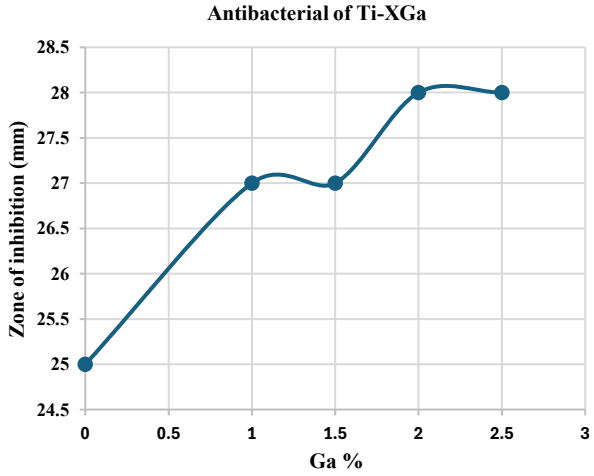


**Figure 5:** Shows the effect of adding Ga to Ti metal on the Zone of inhibition

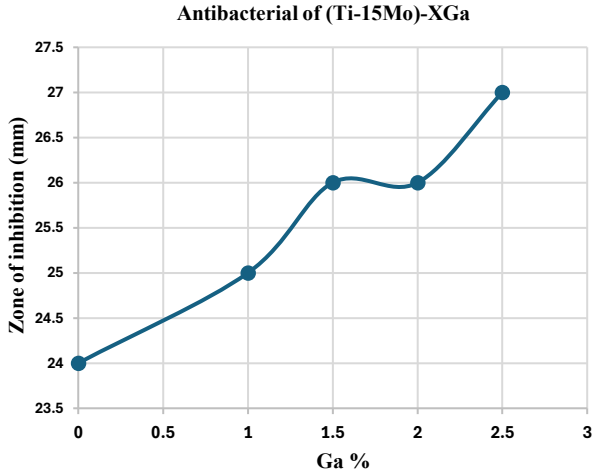


**Figure 6:** Shows the effect of adding Ga to the Ti-15Mo alloy on the Zone of inhibition

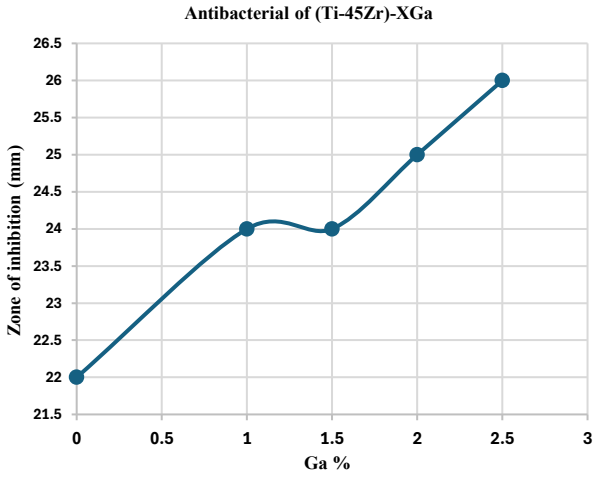


**Figure 7:** Shows the effect of adding Ga to the Ti-45Zr alloy on the Zone of inhibition

Gallium ($Ga^{3+}$) mimics iron ($Fe^{3+}$) due to their similar ionic radii and charge. Bacteria uptake $Ga^{3+}$ via iron transport systems (e.g., siderophores), leading to intracellular iron starvation. $Ga^{3+}$ disrupts iron-dependent enzymes and metabolic pathways (e.g., DNA synthesis, electron transport), inhibiting bacterial growth. Titanium acts as a matrix for controlled release of $Ga^{3+}$ ions, maintaining antibacterial activity over time. Continuous ion release creates a hostile microenvironment for bacteria, preventing colonization. Ga incorporation modifies the $TiO_2$ surface, promoting reactive oxygen species (ROS) generation (e.g., hydroxyl radicals) under light or physiological conditions. Reactive oxygen species (ROS) damage bacterial membranes, proteins, and DNA. Ga inhibits biofilm formation by interfering with bacterial adhesion and quorum sensing. Reduced biofilm resilience enhances susceptibility to antimicrobial agents. Ga alters Titanium's surface charge, hydrophilicity, or nanostructure, promoting physical disruption of bacterial membranes. Direct contact with Ga-doped Ti surfaces damages bacterial cell integrity. Ga doping modifies $TiO_2$'s electrochemical behavior, enhancing ion release or catalytic activity, and improving antibacterial performance without compromising biocompatibility. Table 17 and Figure 6 show the effect of adding gallium to Ti-15Mo alloy in proportions of 1%, 1.5%, 2%, and 2.5% by powder metallurgy method on antibacterial activity (Zone of inhibition). Gallium ($Ga^{3+}$) chemically resembles iron ($Fe^{3+}$), allowing it to disrupt bacterial iron metabolism. Bacteria uptake $Ga^{3+}$ via iron transport systems (e.g., siderophores), leading to intracellular dysfunction.

$Ga^{3+}$ incorporation disrupts iron-dependent enzymes and pathways (e.g., DNA synthesis, electron transport), starving bacteria of essential nutrients. The Ti-15Mo-Ga alloy releases $Ga^{3+}$ ions in a sustained manner in physiological environments. Molybdenum (Mo) enhances the alloy's corrosion resistance, moderating Ga release to avoid cytotoxicity. Continuous low-level $Ga^{3+}$ release creates a bacteriostatic / bactericidal microenvironment without overwhelming host cells. Adding Ga alters the

alloy's surface topography and chemistry, reducing bacterial adhesion. A smoother or more hydrophobic surface prevents bacterial colonization and biofilm formation. Molybdenum (Mo) enhances the alloy's stability and corrosion resistance, ensuring $Ga^{3+}$ release is sustained and localized. The Ti-15Mo matrix acts as a reservoir for $Ga^{3+}$, balancing antibacterial efficacy and biocompatibility. $Ga^{3+}$ ions induce oxidative stress via reactive oxygen species (ROS) generation, damaging bacterial membranes and DNA. ROS-mediated killing complements metabolic disruption, enhancing antibacterial effects.

**Table 17:** Shows the effect of adding Ga to the Ti-15Mo alloy on the Zone of inhibition

| | Sample No. | Zone of inhibition (mm) |
|---|---|---|
| S. aureus | 6 | 24 |
| | 7 | 25 |
| | 8 | 26 |
| | 9 | 26 |
| | 10 | 27 |

Table 18 and Figure 7 show the effect of adding gallium to Ti-45Zr alloy in proportions of 1%, 1.5%, 2%, and 2.5% by powder metallurgy method on antibacterial activity (Zone of inhibition).

**Table 18:** Shows the effect of adding Ga to the Ti-45Zr alloy on the Zone of inhibition

| | Sample No. | Zone of inhibition (mm) |
|---|---|---|
| S. aureus | 11 | 22 |
| | 12 | 24 |
| | 13 | 24 |
| | 14 | 25 |
| | 15 | 26 |

$Ga^{3+}$ ions chemically resemble $Fe^{3+}$, exploiting bacterial iron transport systems (e.g., siderophores). Once internalized, $Ga^{3+}$ disrupts iron-dependent enzymes (e.g., ribonucleotide reductase) critical for DNA synthesis and energy production. Metabolic starvation inhibits bacterial growth and biofilm formation. The Ti-45Zr alloy's stable oxide layer ($TiO_2$-$ZrO_2$) moderates $Ga^{3+}$ release, ensuring sustained antibacterial activity without cytotoxic bursts. Zirconium's corrosion resistance enhances the alloy's durability in physiological environments. Prolonged, localized ion release creates a bacteriostatic microenvironment.

Ga incorporation alters the alloy's surface chemistry and topography. $ZrO_2$ increases hydrophilicity, while Ga creates nanoscale roughness, reducing bacterial adhesion. A smoother, more hydrophilic surface repels bacteria, limiting biofilm formation. Ga-doped $TiO_2$-$ZrO_2$ surfaces generate ROS (e.g., hydroxyl radicals) under physiological conditions, damaging bacterial membranes and DNA. ROS-mediated oxidative stress complements metabolic disruption. Zirconium stabilizes the alloy's passive oxide layer, while Ga provides antibacterial activity. The Ti-45Zr matrix acts as a reservoir for controlled $Ga^{3+}$ release. Balanced mechanical strength, corrosion resistance, and antimicrobial efficacy. Figure 8 shows the Antibacterial activity test of samples against Staphylococcus aureus.

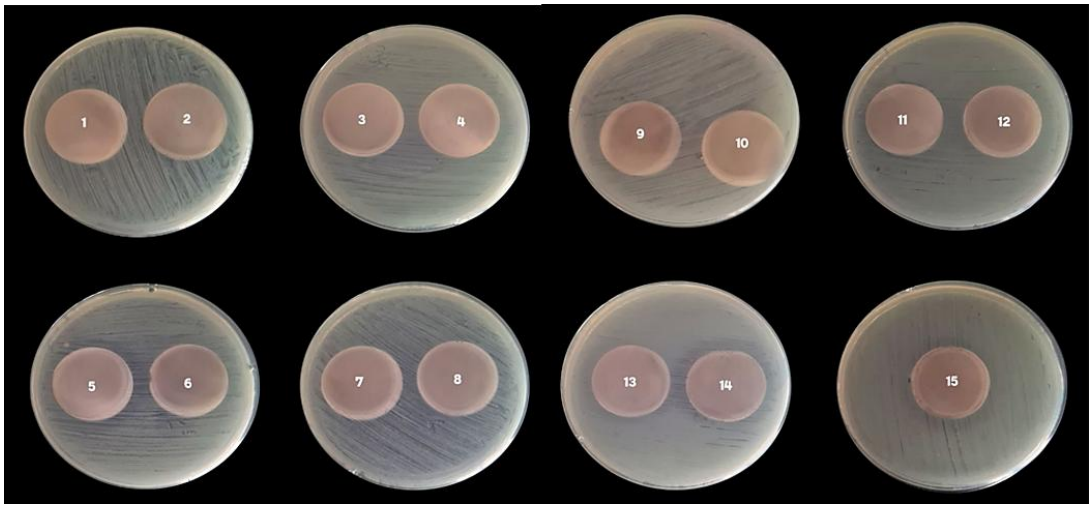


**Figure 8:** Antibacterial activity test of samples against Staphylococcus aureus

## 3.3 MTT assay

Cell survival, proliferation, and differentiation at the implant-host tissue interface are crucial during implantation. Titanium and its alloys have excellent biocompatibility and facilitate cell proliferation. Due to the inert surface and the risk of microbial infection, these biometallic alloys must activate their surface to enhance cell contact and inhibit bacterial growth. The cellular

response to biomaterial surfaces is considered a fundamental criterion for assessing material biocompatibility. Figure 9 shows control untreated MCF-10 cells before being treated with samples.

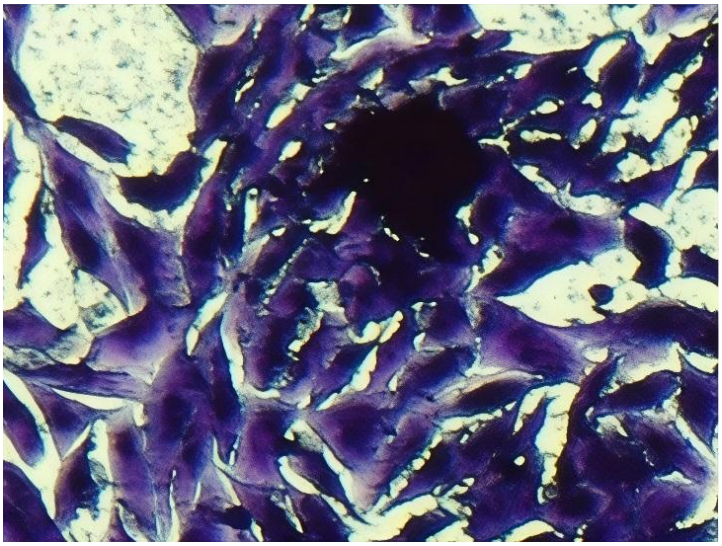

**Figure 9:** Control untreated MCF-10 cells with samples (40x)

The antiproliferative activity (anticancer activity) of sample 3 against MCF-10 cells was studied using an MTT assay. As shown in Table 19 and Figures 10, the results demonstrate that sample 3 has biocompatibility properties for MCF-10 cells.

**Table 19:** Cytotoxicity in triplicate of Ti-1.5Ga alloy

| Concentration (µg/ml) | Cytotoxicity (%) for A | Cytotoxicity (%) for B | Cytotoxicity (%) for C |
|---|---|---|---|
| 0 | 0 | 0 | 0 |
| 12.5 | 3.25 | 2.35 | 0.98 |
| 25 | 6.35 | 5.98 | 6.35 |
| 50 | 8.36 | 10.25 | 7.58 |
| 100 | 11.23 | 10.54 | 9.58 |

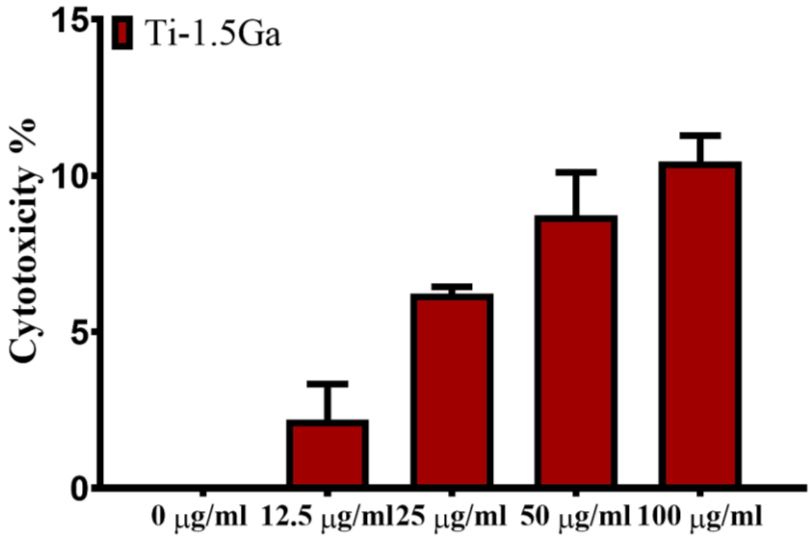


**Figure 10:** Cytotoxicity effect of sample 3 in MCF-10 cells

The bar chart illustrates the cytotoxic effect (%) of the Ti-1.5Ga alloy on MCF-10 cells at increasing concentrations: 0 ,12.5 , ,50 ,25and 100 µg/ml. At 0 µg/ml (control untreated), cytotoxicity is 0%. As expected, no toxicity was observed without the alloy serving as a baseline. At 12.5 µg/ml, cytotoxicity is ~2%, indicating minimal toxicity at low concentrations and high biocompatibility. At 25 µg/ml, cytotoxicity is ~6%, a Moderate increase but still considered biocompatible (under 10% is often acceptable). At 50 µg/ml, cytotoxicity is ~9%, approaching the threshold where mild cytotoxic effects are observed. At 100 µg/ml, cytotoxicity is ~10.5%, the highest observed cytotoxic effect, but still within a relatively low range of cytotoxicity.

The SEM examination for morphological changes in MCF-10 cells after being treated with Ti-1.5Ga didn't demonstrate any cytotoxic impacts of the samples against MCF-10 cells. It wasn't caused by cell shape changes, cell size reduction, cell clustering, reduced cell extensions, and shrinkage of nuclei, as shown in Figure 11. The Ti-1.5Ga alloy shows low to moderate cytotoxicity in MCF-10 cells. It is generally biocompatible up to 50 µg/ml, with slight cytotoxic effects at 100 µg/ml. These results suggest

it is a promising biomaterial with good tolerance at low-to-moderate doses, potentially suitable for implantable or biomedical applications.

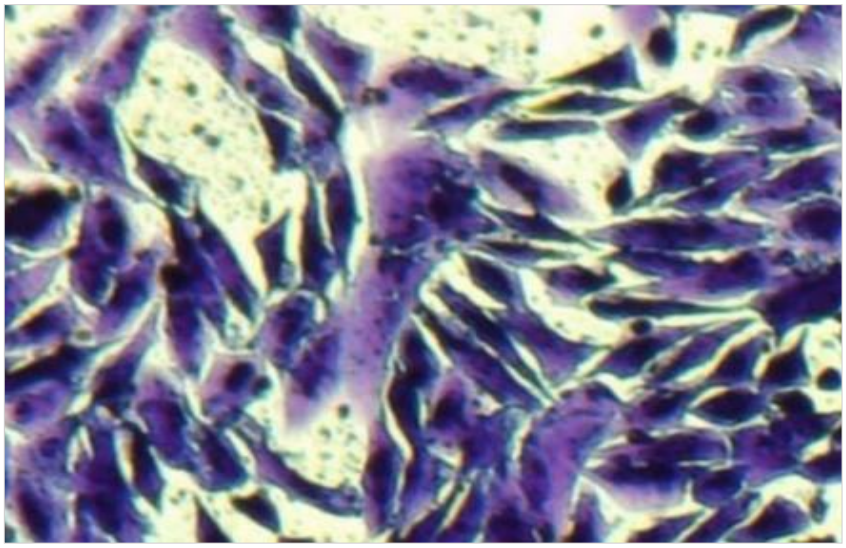

**Figure 11:** Morphological changes in MCF-10 cells after being treated with sample 3 (40x)

The antiproliferative activity (anticancer activity) of sample 9 against MCF-10 cells was studied using an MTT assay. As shown in Table 20 and Figures 12, the results demonstrate that sample 9 has biocompatibility properties for MCF-10 cells.

**Table 20:** Cytotoxicity in triplicate of (Ti-15Mo)-2Ga alloy

| Concentration (µg/ml) | Cytotoxicity (%) for A | Cytotoxicity (%) for B | Cytotoxicity (%) for C |
|---|---|---|---|
| 0 | 0 | 0 | 0 |
| 12.5 | 3.25 | 1.95 | 2.20 |
| 25 | 5.28 | 6.33 | 4.25 |
| 50 | 8.96 | 9.47 | 10.35 |
| 100 | 11.35 | 10.58 | 11.25 |

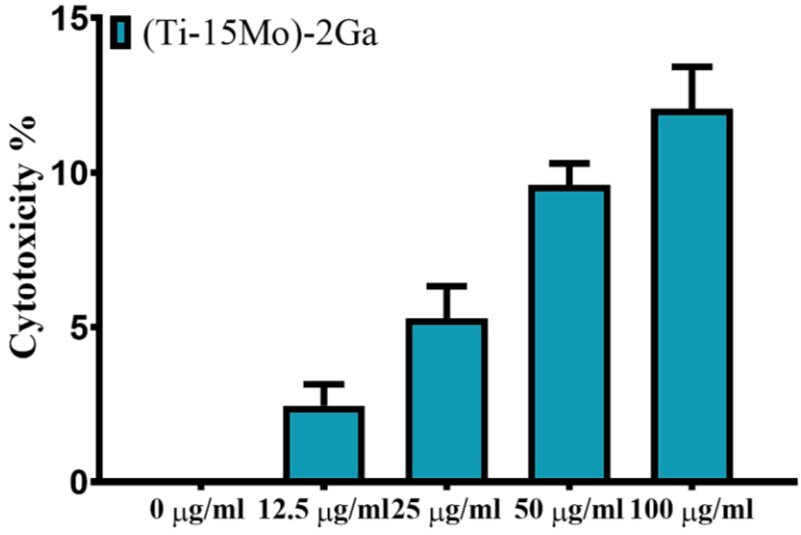


**Figure 12:** Cytotoxicity effect of sample 9 in MCF-10 cells

The bar chart illustrates the cytotoxic effect (%) of the (Ti-15Mo)-2Ga alloy on MCF-10 cells at increasing concentrations: 0, 12.5, 25, 50, and 100 µg/ml. At 0 µg/ml (control untreated), cytotoxicity is 0%. As expected, no toxicity was observed without the alloy serving as a baseline. At 12.5 µg/ml, cytotoxicity is ~2.5%, Minimal toxicity, suggesting good biocompatibility at low dose. At 25 µg/ml, cytotoxicity is ~5.5%, still within a biocompatible range, but the effect is starting to appear. At 50 µg/ml, cytotoxicity is ~9.5%, with moderate toxicity; this may begin to affect sensitive cells. 100 µg/ml, cytotoxicity is ~11%, the highest toxicity observed, but still within a relatively low cytotoxicity range.

The SEM examination for morphological changes in MCF-10 cells after being treated with (Ti-15Mo)-2Ga hasn't demonstrated any cytotoxic impacts of samples against MCF-10 cells and wasn't caused by cell shape changes, cell size reduction, cell clustering, reduced cell extensions, and shrinkage of nuclei, as shown in Figure 13. The (Ti-15Mo)-2Ga alloy

shows low to moderate cytotoxicity in MCF-10 cells. It is generally biocompatible up to 50 µg/ml, with slight cytotoxic effects at 100 µg/ml. The alloy shows low cytotoxicity overall and maintains acceptable biocompatibility up to moderate concentrations. This makes it a promising candidate for biomedical applications (implants and coatings).

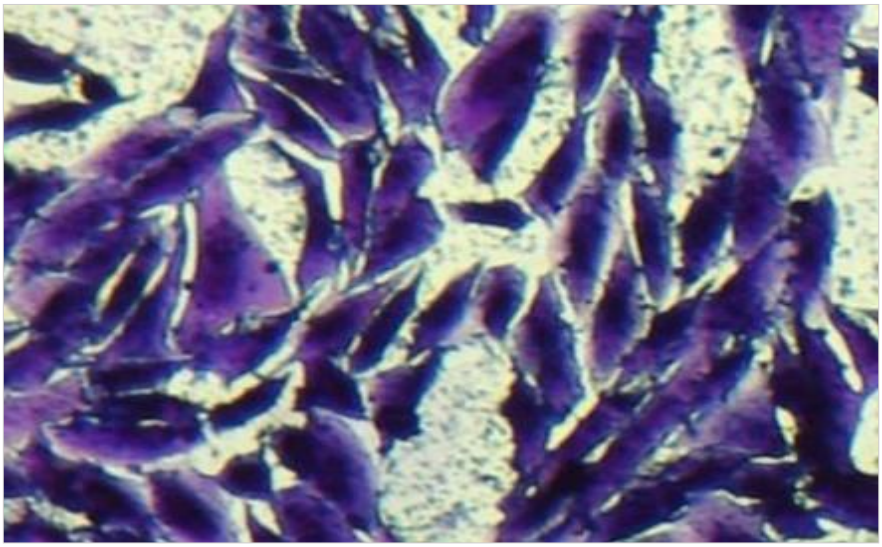

**Figure 13:** Morphological changes in MCF-10 cells after being treated with sample 9 (40x)

The antiproliferative activity (anticancer activity) of sample 14 against MCF-10 cells was studied using an MTT assay. As shown in Table 21 and Figures 14, the results demonstrate that sample 14 has biocompatibility properties for MCF-10 cells.

**Table 21:** Cytotoxicity in triplicate of (Ti-45Zr)-2Ga alloy

| Concentration (µg/ml) | Cytotoxicity (%) for A | Cytotoxicity (%) for B | Cytotoxicity (%) for C |
|---|---|---|---|
| 0 | 0 | 0 | 0 |
| 12.5 | 2.54 | 1.58 | 3.65 |
| 25 | 6.35 | 4.50 | 3.69 |
| 50 | 10.55 | 8.46 | 11.58 |
| 100 | 11.25 | 12.50 | 9.88 |

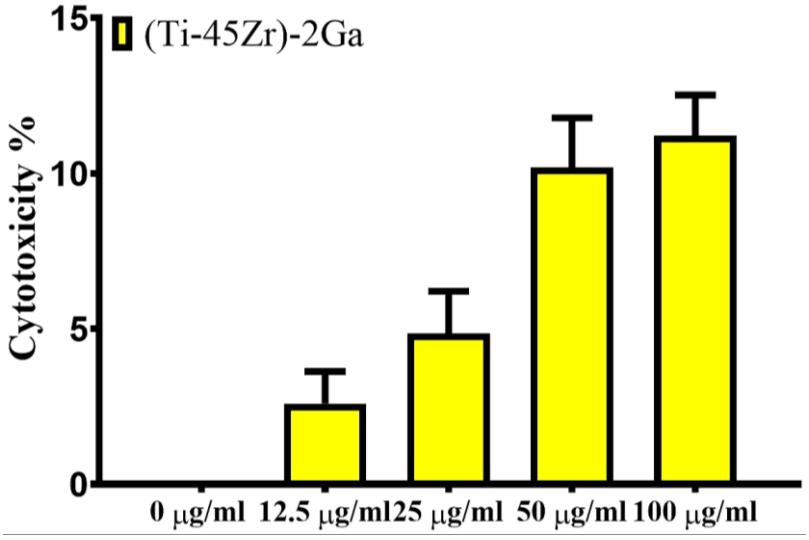


**Figure 14:** Cytotoxicity effect of sample 14 in MCF-10 cells

The bar chart shows the alloy's cytotoxic effect (%) (Ti-45Zr)-2Ga on MCF-10 cells across concentrations: 0, 12.5, 25, 50, and 100 µg/ml. At 0 µg/ml (control untreated), cytotoxicity is 0%. As expected, no toxicity was observed without the alloy serving as a baseline. At 12.5 µg/ml, cytotoxicity is ~2.5%, which is very low. At 25 µg/ml, cytotoxicity is ~5%, still in the acceptable range for biomedical use. At 50 µg/ml, cytotoxicity is ~10%, mild cytotoxic effect; moderate concern. At 100 µg/ml, cytotoxicity is ~11%, the highest toxicity observed, but still within a relatively low cytotoxicity range.

The SEM examination for morphological changes in MCF-10 cells after treatment with (Ti-45Zr)-2Ga didn't demonstrate any cytotoxic impacts of the samples against MCF-10 cells. It wasn't caused by cell shape changes, cell size reduction, cell clustering, reduced cell extensions, and shrinkage of nuclei, as shown in Figure 15. (Ti-45Zr)-2Ga shows low to moderate

cytotoxicity depending on the concentration. It is generally biocompatible up to 50 µg/ml, with slight cytotoxic effects at 100 µg/ml. These results suggest the alloy is biocompatible and potentially useful in biomedical devices.

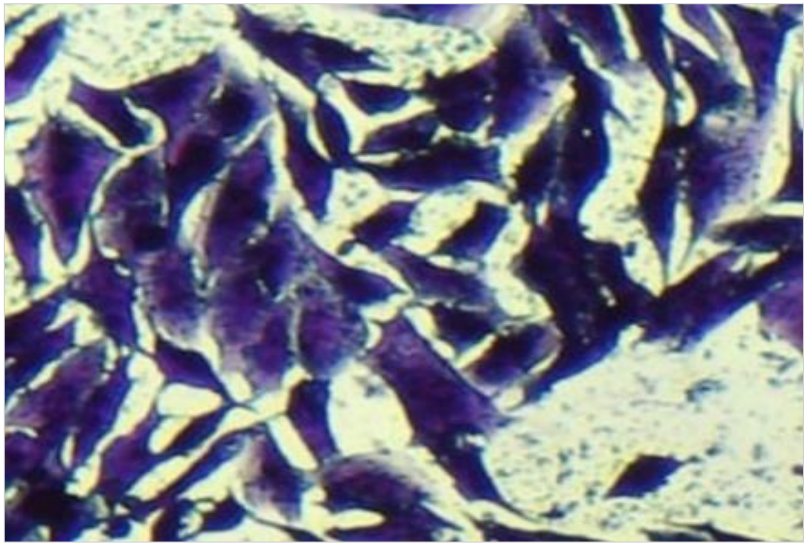

**Figure 15:** Morphological changes in MCF-10 cells after being treated with sample 14 (40x)

Most tested alloys showed low or acceptable cytotoxicity at low concentrations (12.5–25 µg/ml). They showed excellent biological performance with less than 10% toxicity, even at a concentration of (50 µg/ml). Increasing gallium content to 2% increased the cytotoxicity of the (Ti-15Mo)-2Ga and (Ti-45Zr)-2Ga alloys at a concentration of (100 µg/ml) but remained within acceptable limits. Titanium and its alloys are attracting considerable attention as prospective candidates for developing next-generation metallic biomaterials, especially for hard tissue implant applications, owing to their exceptional mechanical properties and biocompatibility. Subtle integration with bactericidal agents is a viable method for augmenting antibacterial properties [29]. This study examined the effect of minor gallium (Ga) incorporation into Ti, Ti-15Mo, and their alloys on the antibacterial efficacy against S. aureus, a prevalent etiological agent linked to the aseptic failure of implanted orthopedic devices, as well as its antiproliferative effects (anticancer activity) or cytotoxicity following Ga addition [30]. This study shows that elevated Ga concentrations markedly reduced S. aureus survivability in comparison to the clinically utilized cp-Ti, Ti-15Mo, and Ti-45Zr, for numerous reasons that will be elaborated upon below:

1) Gallium ($Ga^{3+}$) mimics iron ($Fe^{3+}$) due to their similar ionic radii and charge, allowing it to disrupt bacterial iron metabolism. Bacteria uptake $Ga^{3+}$ via iron transport systems (e.g., siderophores), leading to intracellular iron starvation. $Ga^{3+}$ disrupts iron-dependent enzymes and metabolic pathways (e.g., DNA synthesis, electron transport), inhibiting bacterial growth and biofilm formation [31].
2) The Ti, Ti-15Mo, and Ti-45Zr alloys' stable oxide layers, $TiO_2$, $TiO_2$-$MoO_2$, and $TiO_2$-$ZrO_2$, moderate $Ga^{3+}$ release, ensuring sustained antibacterial activity without cytotoxic bursts. Ti, Ti-15Mo, and Ti-Zr act as a matrix for controlled release of $Ga^{3+}$ ions, maintaining antibacterial activity over time. Continuous ion release creates a hostile microenvironment for bacteria, preventing colonization [32].
3) Titanium, Molybdenum, Zirconium, and Gallium enhance the alloy's corrosion resistance, moderating Ga release to avoid cytotoxicity. Continuous low-level $Ga^{3+}$ release creates a bacteriostatic/bactericidal microenvironment without overwhelming host cells [33].
4) Ga incorporation modifies the $TiO_2$ surface, promoting reactive oxygen species (ROS) generation (e.g., hydroxyl radicals) under light or physiological conditions. Reactive oxygen species (ROS) damage bacterial membranes, proteins, and DNA [34].
5) $Ga^{3+}$ ions induce oxidative stress via reactive oxygen species (ROS) generation, damaging bacterial membranes and DNA. ROS-mediated killing complements metabolic disruption, enhancing antibacterial effects [35].
6) Adding Ga alters the alloy's surface topography and chemistry, reducing bacterial adhesion. A smoother or more hydrophobic surface prevents bacterial colonization and biofilm formation [36].
7) Ga inhibits biofilm formation by interfering with bacterial adhesion and quorum sensing. Reduced biofilm resilience enhances susceptibility to antimicrobial agents. Ga alters Titanium's surface charge, hydrophilicity, or nanostructure, promoting physical disruption of bacterial membranes. Direct contact with Ga-doped Ti surfaces damages bacterial cell integrity [37].
8) Samples (3, 9, and 14) exhibited higher antiproliferative activity (anticancer activity) against MCF-10 cells with concentration-dependent cytotoxicity. SEM examination didn't demonstrate any cytotoxic impacts of samples (3, 9, and 14) against MCF-10 cells. It wasn't caused by cell shape changes, cell size reduction, cell clustering, reduced cell extensions, and shrinkage of nuclei, and has biocompatibility properties [38].

## 4. Conclusion

1) Adding Ga in different proportions led to the emergence of transformations in the metallic phases and intermetallic compounds, as it was observed that it resulted in transitions of metallic phases from α to α' and the emergence of intermetallic compounds such as $Ti_5Ga_3$ or $Ti_3Ga$ in Ti metal, increased the stability of the β phase and the emergence of intermetallic compounds such as $Ti_5Ga_3$, $Ti_5Ga_4$, and $Ti_3Ga$ in Ti-15Mo alloy, and resulted in transitions of metallic phases from α to β in Ti-45Zr alloy.
2) Adding Ga increased the antibacterial activity of the samples with the highest antibacterial activity occurring at 2.5% Ga, as it was observed that it increased the Zone of inhibition of Ti metal from (25 mm) to (28 mm) by about (12%), increased the Zone of inhibition of Ti-15Mo alloy from (24 mm) to (27 mm) by about (12.5%), and increased the Zone of inhibition of Ti-45Zr alloy from (22 mm) to (26 mm) by about (18%). This was because the $Ga^{3+}$ ions released from the samples exhibit strong antibacterial activity against bacteria such as Acinetobacter baumannii and Staphylococcus aureus.
3) Low cytotoxicity to MCF-10 was recorded at low concentrations up to 50 µg/ml for all samples and gradually increased with increasing concentration up to 100 µg/ml due to the potential of $Ga^{3+}$ ions release. The increase in Ga led to increased cytotoxicity, but it remained within acceptable limits. This makes all samples promising candidates for biomaterials applications.

### Author contributions

Conceptualization, **A. Hasan**, **F. Al-Hasani,** and **E. Al-Hassani**; data curation, **A. Hasan**; formal analysis, **A. Hasan**; investigation, **A. Hasan**; methodology, **A. Hasan**; project administration, **A. Hasan**; resources, **A. Hasan**; software, **A. Hasan**; supervision, **F. Al-Hasani**, and **E. Al-hassani**; validation, **A. Hasan, F. Al-Hasani, and E. Al-Hassani**; visualization, **A. Hasan**; writing—original draft preparation, **A. Hasan**; writing—review and editing, **A. Hasan**. All authors have read and agreed to the published version of the manuscript.

### Funding

This research received no specific grant from any funding agency in the public, commercial, or not-for-profit sectors.

### Data availability statement

The data that support the findings of this study are available on request from the corresponding author.

### Conflicts of interest

The authors declare that there is no conflict of interest.

## References

**[1]** Z. Guo, Y. Huang, C. Sun, Z. He, D. Yuan, B. Cai, et al., Ti–Mo–Zr alloys for bone repair: mechanical properties, corrosion resistance, and biological performance, J. Mater. Res. Technol., 24 (2023) 7624-7637. https://doi.org/10.1016/j.jmrt.2023.05.006

**[2]** M. A. Hussein, M. A., Azeem, A. M. Kumar, S. Saravanan, N. Ankah, et. al., Design and processing of near-β Ti–Nb–Ag alloy with low elastic modulus and enhanced corrosion resistance for orthopedic implants, J. Mater. Res. Technol., 24 (2023) 259-273. https://doi.org/10.1016/j.jmrt.2023.03.003

**[3]** E. dos S. Monteiro, F. M. de Souza Soares, L. F. Nunes, A. I. Carvalho Santana, R. S. Sergio de Biasi, C. N. Elias, Comparison of the wettability and corrosion resistance of two biomedical Ti alloys free of toxic elements with those of the commercial ASTM F136 (Ti–6Al–4V) alloy, J. Mater. Res. Technol., 9 (2020) 16329-16338. http://dx.doi.org/10.1016/j.jmrt.2020.11.068

**[4]** J. G. S. Souza, M. M. Bertolini, R. C. Costa, B. E. Nagay, A. Dongari-Bagtzoglou, V. A. R. Barão, Targeting implant-associated infections: titanium surface loaded with antimicrobial, IScience, 24 (2021) 102008. http://dx.doi.org/10.1016/j.isci.2020.102008

**[5]** K. S. Malchau, J. Tillander, M. Zaborowska, M. Hoffman, I. Lasa, P. Thomsen, et al., Biofilm properties in relation to treatment outcome in patients with first-time periprosthetic hip or knee joint infection, J. Orthop. Translat., 30 (2021) 31-40. http://dx.doi.org/10.1016/j.jot.2021.05.008

**[6]** F. J. Al-Hasani, E. S. Al-Hassani, Preparation and Characterization of Antimicrobial Wound Healing Materials from Natural Origins, J. Phys.: Conf. Ser., 2857 (2024) 012028. http://dx.doi.org/10.1088/1742-6596/2857/1/012028

**[7]** S. Hijazi, D. Visaggio, M. Pirolo, E. Frangipani, L. Bernstein, P. Visca, Antimicrobial activity of gallium compounds on ESKAPE pathogens, Front. Cell. Infect. Microbiol., 8 (2018) 316. https://doi.org/10.3389/fcimb.2018.00316

**[8]** C. H. Goss, Y. Kaneko, L. Khuu, G. D. Anderson, S. Ravishankar, et al., Gallium disrupts bacterial iron metabolism and has therapeutic effects in mice and humans with lung infections, Sci. Transl. Med., 10 (2018) 7520. https://doi.org/10.1126/scitranslmed.aat7520

**[9]** F. Minandri, C. Bonchi, E. Frangipani, F. Imperi, P. Visca, Promises and failures of gallium as an antibacterial agent, Future Microbiol., 9 (2014) 379-397. https://doi.org/10.2217/fmb.14.3

**[10]** M. Kaur, and K. Singh, Review on Titanium and Titanium based alloys as biomaterials for orthopedic applications, Mater. Sci. Eng.,: C, 102 (2019) 844-862. https://doi.org/10.1016/j.msec.2019.04.064

**[11]** S. Yamaguchi, S. Nath, Y. Sugawara, D. Divakarla, T. Das, J. Manos, Two-in-one biointerfaces—Antimicrobial and bioactive nanoporous gallium titanate layers for titanium implants, Nanomaterials, 7 (2017) 229. https://doi.org/10.3390/nano7080229

**[12]** A. Cochis, B. Azzimonti, R. Chiesa, L. Rimondini, M. Gasik, Metallurgical gallium additions to titanium alloys demonstrate a strong time-increasing antibacterial activity without any cellular toxicity, ACS ACS Biomater. Sci. Eng.,ACS, 5 (2019) 2815-2820. https://doi.org/10.1021/acsbiomaterials.9b00147

**[13]** J. Vishnu, L. A. Alberta, A. Hariharan, S. Pilz, et al., Novel low modulus beta-type Ti-Nb alloys by gallium and copper minor additions for antibacterial implant applications, J. Mater. Res. Technol., 20 (2022) 3306-3322. https://doi.org/10.1016/j.jmrt.2022.08.111

**[14]** L. A. Alberta, J. Vishnu, A. Hariharan, Pilz, S., et al., Novel low modulus beta-type Ti–Nb alloys by gallium and copper minor additions for antibacterial implant applications, J. Mater. Res. Technol., 20 (2022) 3306-3322. https://doi.org/10.1016/j.jmrt.2022.08.111

**[15]** R. McHendrie, W. Xiao, V. K. Truong, R. Hashemi, Gallium-Containing Materials and Their Potential within New-Generation Titanium Alloys for Biomedical Applications, Biomimetics, 8 (2023) 573. https://doi.org/10.3390/biomimetics8080573

**[16]** F. Li, K. Huang, J. Wang, K. Yuan, Y. Yang, Y. Liu, et al., A dual functional Ti-Ga alloy: inhibiting biofilm formation and osteoclastogenesis differentiation via disturbing iron metabolism, Biomater. Res., 27 (2023) 24. https://doi.org/10.1186/s40824-023-00362-1

**[17]** H. H. Bahjat, R. A. Ismail, G. M. Sulaiman, and M. S. Jabir, Magnetic field-assisted laser ablation of titanium dioxide nanoparticles in water for anti-bacterial applications, J. Inorg. Organomet. Polym. Mater., (2020) 1-8. https://doi.org/10.21203/rs.3.rs-176836/v1

**[18]** K. S. Khashan, F. A. Abdulameer, M. S. Jabir, A. A. Hadi, and G. M. Sulaiman, Anticancer activity and toxicity of carbon nanoparticles produced by pulsed laser ablation of graphite in water, Adv. Nat. Sci: Nanosci. Nanotechnol., 11 (2020) 035010. http://dx.doi.org/10.1088/2043-6254/aba1de

**[19]** K. S. Khashan, B. A. Badr, G. M. Sulaiman, M. S. Jabir, and S. A. Hussain, Antibacterial activity of Zinc Oxide nanostructured materials synthesis by laser ablation method, 2nd International Conference on Materials, Laser science and Applied physics, 1795, 2021, 01204. http://dx.doi.org/10.1088/1742-6596/1795/1/012040

**[20]** M. A. Jihad, F. Noori, M. S. Jabir, S. Albukhaty, F. A. AlMalki, and A. A. Alyamani, Polyethylene Glycol Functionalized Graphene Oxide Nanoparticles Loaded with Nigella sativa Extract: A Smart Antibacterial Therapeutic Drug Delivery System, Molecules, 26 (2021) 3067. https://doi.org/10.3390/molecules26113067

**[21]** M. K. Mohammed, M. R. Mohammad, M. S. Jabir, and D. S. Ahmed, Functionalization, characterization, and antibacterial activity of single wall and multi wall carbon nanotubes, 1st International Conference in Physical Science and Advance Materials, 757, 2021, 012028. http://dx.doi.org/10.1088/1757-899X/757/1/012028

**[22]** H. N. K. Al Salman, E. T. Ali, M. Jabir, G. M. Sulaiman, and S. A. Al Jadaan, Benzhydrylsulfinyl N hydroxyacetamide Na extracted from fig as a novel cytotoxic and apoptosis inducer in A549 and AMJ 13 cell lines via P53 and caspase 8 pathway, Eur. Food Res. Technol., 246 (2020) 1591–1608. https://doi.org/10.1007/s00217-020-03515-x

**[23]** A. J. Jasim, G. M. Sulaiman, H. Ay, S. A. Mohammed, H. A. Mohammed, M. S. Jabir, et. al., Preliminary trials of the gold nanoparticles conjugated chrysin: An assessment of antioxidant, antimicrobial, and in vitro cytotoxic activities of a nanoformulated flavonoid, Nanotechnol. Rev., 11 (2022) 2726-2741. http://dx.doi.org/10.1515/ntrev-2022-0153

**[24]** M. Jawad, K. Öztürk, and M. S. Jabir, TNF-α loaded on gold nanoparticles as promising drug delivery system against proliferation of breast cancer cells, Mater. Today Proc., 42 (2021) 3057-3061. https://doi.org/10.1016/j.matpr.2020.12.836

**[25]** A. A. Alyamani, M. H. Al-Musawi, S. Albukhaty, G. M. Sulaiman, K. M. Ibrahim, et al., Electrospun polycaprolactone/chitosan nanofibers containing cordia myxa fruit extract as potential biocompatible antibacterial wound dressings, Molecules, 28 (2023) 2501. https://doi.org/10.3390/molecules28062501

**[26]** A. A. Ibrahim, M. M. Kareem, T. H. Al-Noor, T. Al-Muhimeed, A. A. AlObaid, et al., Pt (II)-Thiocarbohydrazone complex as cytotoxic agent and apoptosis inducer in Caov-3 and HT-29 cells through the P53 and Caspase-8 pathways, Pharmaceuticals, 14 (2021) 509. https://doi.org/10.3390/ph14060509

**[27]** M. S. Jabir, N. A. Abood, M. H. Jawad, K. Öztürk, H. Kadhim, et al., Gold nanoparticles loaded TNF-α and CALNN peptide as a drug delivery system and promising therapeutic agent for breast cancer cells, Mater. Technol., 37 (2022) 3152-3166. http://dx.doi.org/10.1080/10667857.2022.2133073

**[28]** Z. S. Abbas, G. M. Sulaiman, M. S.Jabir, S. A.Mohammed, R. A. Khan, H. A.Mohammed, and A. Al-Subaiyel, Galangin/β-Cyclodextrin Inclusion Complex as a Drug-Delivery System for Improved Solubility and Biocompatibility in Breast Cancer Treatment, Molecules, 27 (2022) 4521. https://doi.org/10.3390/molecules27144521

**[29]** M. Calin, A. Helth, J. J. G. Moreno, M. Bönisch, V. Brackmann, et al., Elastic softening of β-type Ti–Nb alloys by indium (In) additions, J. Mech. Behav. Biomed. Mater., 39 (2014) 162-174. https://doi.org/10.1016/j.jmbbm.2014.07.010

**[30]** N. Benito, I. Mur, A. Ribera, A. Soriano, D. Rodríguez-Pardo, The different microbial etiology of prosthetic joint infections according to route of acquisition and time after prosthesis implantation, including the role of multidrug-resistant organisms, J. Clin. Med. Res., 8 (2019) 673. http://dx.doi.org/10.3390/jcm8050673

**[31]** F. Li, K. Huang, J. Wang, K. Yuan, Y. Yang, Y., Liu, et. al., A dual functional Ti-Ga alloy: inhibiting biofilm formation and osteoclastogenesis differentiation via disturbing iron metabolism, Biomater. Res., 27 (2022) 24. http://dx.doi.org/10.21203/rs.3.rs-2265733/v1

**[32]** S. Hijazi, D. Visaggio, M. Pirolo, E. Frangipani, L.Bernstein, et. al., Antimicrobial activity of gallium compounds on ESKAPE pathogens, Front. Cell. Infect. Microbiol., 8 (2018) 316. https://doi.org/10.3389/fcimb.2018.00316

**[33]** A. Akman, L. A. Alberta, P. M. Giraldo-Osorno, A. B. Turner, M. Hantusch, et. al., Effect of minor gallium addition on corrosion, passivity, and antibacterial behaviour of novel β-type Ti–Nb alloys, J. Mater. Res. Technol., 25 (2023) 4110-4124. https://doi.org/10.1016/j.jmrt.2023.06.219

**[34]** C. H. Goss, Y. Kaneko, L. Khuu, G. D. Anderson, S. Ravishankar, et. al., Gallium disrupts bacterial iron metabolism and has therapeutic effects in mice and humans with lung infections, Sci Transl Med., 10 (2018) 7520. https://doi.org/10.1126/scitranslmed.aat7520

**[35]** A. H. Hashem, M. A. Abdel-Maksoud, S. Fatima, S. M. Almutairi, M. A. Ghorab, et. al., Synthesis and characterization of innovative GA@ Ag-CuO nanocomposite with potent antimicrobial and anticancer properties, Sci. Rep., 15 (2025) 689. https://doi.org/10.1038/s41598-024-76446-2

**[36]** I. S. Geljic, N. Melis, F. Boukhechba, S. Schaub, C. Mellier, et. al., Gallium enhances reconstructive properties of a calcium phosphate bone biomaterial, J. Tissue. Eng. Regen. Med., 12 (2018) e854-e866. https://doi.org/10.1002/term.2396

**[37]** F. Minandri, C. Bonchi, E. Frangipani, F. Imperi, P. Visca, Promises and failures of gallium as an antibacterial agent, Future Microbiol., 9 (2014) 379-397. https://doi.org/10.2217/fmb.14.3

**[38]** A. J. Jasim, G. M. Sulaiman, H. Ay, S. A. Mohammed, H. A. Mohammed, et. al., Preliminary trials of the gold nanoparticles conjugated chrysin: An assessment of anti-oxidant, antimicrobial, and in vitro cytotoxic activities of a nanoformulated flavonoid, Nanotechnol. Rev., 11 (2022) 2726-2741. http://dx.doi.org/10.1515/ntrev-2022-0153